Paper No.
7861

NACE INTERNATIONAL CORROSION 2016 CONFERENCE & EXPO

Slow Strain Rate and Rising Step Load Hydrogen Embrittlement Testing of UNS N07718

Brian Kagay
Colorado School of Mines
1500 Illinois St.
Golden, CO, 80401
USA

Kip Findley
Colorado School of Mines
1500 Illinois St.
Golden, CO, 80401
USA

Steve Coryell
Special Metals Corporation
3200 Riverside Dr
Huntington, WV, 25705
USA

Andrew Nissan
Chevron Corporation
100 Chevron Way
Richmond, CA, 94802
USA

ABSTRACT

The influence of testing methods and microstructure on hydrogen embrittlement susceptibility of UNS[(1)] N07718 was assessed through slow strain rate (SSR) experiments and rising step load (RSL) testing performed in air and in a cathodic hydrogen charging test cell. The alloy was annealed and either peak-aged or over-aged to produce different strengths and precipitation conditions. The change in ductility, strength, and threshold stress intensity factor for crack growth due to hydrogen charging are compared. Over-aging resulted in superior SSR ductility ratios and higher threshold stress intensity factors compared to peak-aging. The better performance of the over-aged condition occurred despite more δ phase present at the grain boundaries, which indicates an influence of γ' and γ" precipitation on hydrogen embrittlement resistance. Both conditions exhibited mixtures of intergranular and transgranular fracture in the embrittled region for both the SSR and RSL tests.

Key words: Precipitation hardened nickel-base alloys, Hydrogen embrittlement, Slow strain rate testing, Rising step load testing, UNS N07718

INTRODUCTION

UNS N07718, hereafter referred to as alloy 718, is one of several nickel-base corrosion resistant alloys (CRAs) from which components used for deep-sea wells in the oil and gas industry are produced. Packers, tubing hangers, fasteners, and bolting components are all fabricated from CRAs because of their high-strength and resistance to general corrosion processes. Field failures of CRA components

(1) Unified Numbering System for Metals and Alloys (UNS), SAE International, Warrendale, PA, and ASTM International, West Conshohocken, PA

can occur due to hydrogen embrittlement caused by the uptake of atomic hydrogen, which may be produced in several different ways in downhole environments.[1–5] In these cases, hydrogen embrittlement is an environmental cracking process by which atomic hydrogen is adsorbed on the surface and diffuses into the alloy, resulting in a decrease in plasticity and/or fracture strength.

Slow strain rate (SSR) tension testing of alloys under cathodic polarization is the most common testing method to determine a material's susceptibility to hydrogen embrittlement in such environments. Hydrogen embrittlement testing of CRAs used in deep-sea wells normally involves electrolytic charging of a specimen in solution to simulate galvanic coupling or cathodic protection either before or during a SSR tensile test. Ratios of the results of the tests (total elongation, reduction in area, yield strength, notched tensile strength) from the simulated environment and an inert environment are compared for different alloys to determine relative susceptibilities for those alloys.[6,7] SSR tensile testing is a preferred method for evaluating alloy susceptibility to hydrogen embrittlement due to the relatively short test times.[8]

Many studies have evaluated the susceptibility of nickel-base CRAs to hydrogen embrittlement.[1,3,9–19] These studies have used a variety of different testing parameters (strain rate, solution, electrolytic charging current density or potential, and temperature), which can make it difficult to compare results from one study to another. Besides strain rate and environmental testing parameters, there are other not commonly reported factors that can affect measured hydrogen embrittlement susceptibility. For smooth specimens, the surface finish can affect the results in the simulated environment;[8] polishing decreases the influence of surface flaws on crack initiation. The rigidity of the tensile frame can also influence the results of SSR testing. When a test is performed at a constant displacement rate, the actual strain rate of the specimen, particularly in the elastic regime, is dependent on the compliance of the tensile frame. A less rigid frame results in a slower strain rate for a given displacement rate. Slower strain rates can result in a decrease in mechanical properties in hydrogen environments.[20] Variations in hydrogen embrittlement susceptibility ratios may also occur because there is a larger stress driving crack propagation for alloys with higher strengths. The stress imposed on cracks during plastic deformation depends on the yield stress and work hardening rate of the alloys.

Fracture mechanics testing is a potential alternative to SSR tension testing because the result is a material fracture property that is relevant for design purposes.[21] Constant displacement or constant load fracture mechanics testing of pre-cracked specimens is conventionally used to simulate service conditions, but the long test durations (as long as 30 days for Ni-base alloys) make it difficult to efficiently evaluate multiple alloys, microstructures, and environmental conditions. Methods for performing accelerated fracture mechanics tests to assess hydrogen embrittlement while still determining sufficiently conservative fracture mechanics properties have been developed, including rising step load (RSL) testing and constant displacement rate tests.

The RSL test, also known as the incremental step loading technique in ASTM[(2)] F1624,[22] is a type of accelerated fracture mechanics test that can be used to evaluate hydrogen embrittlement susceptibility and determine threshold stress intensity factors (K_{th}) for crack propagation of a specimen tested with cathodic polarization. Ratios of K_{th} from specimens tested with cathodic polarization versus an inert environment can also be used to compare hydrogen susceptibilities between alloys. A schematic of a load versus time plot for an RSL test is shown in Figure 1. The test is performed by first loading a notched specimen to a predetermined value. When the load reaches the specified value, the specimen is held at a constant displacement for a predetermined amount of time.[22] After the hold time, the load on the specimen is increased by the same amount as the first loading step and again held at constant displacement for the same amount of time. In this paper, the load increase in each step will be referred to as the step size and the hold time at constant displacement will be called the step time. In Figure 1, the curves have step sizes of 2000 lb (8,900 N) and 1,000 lb (4,450 N) and a step time of 2 h. The load on the specimen is incrementally increased in this manner until environmentally-induced crack growth occurs, which results in a load drop. The loads associated with the step previous to where cracking

[(2)] ASTM International, 100 Barr Harbor Drive, West Conshohocken, PA, 19428

occurred are used to determine K_{th} for crack growth in the testing environment.[21,22] ASTM F1624 provides guidelines for determining the step sizes and step times for steels, but nickel-base alloys may require longer hold times due to the much lower diffusivity of hydrogen in nickel.

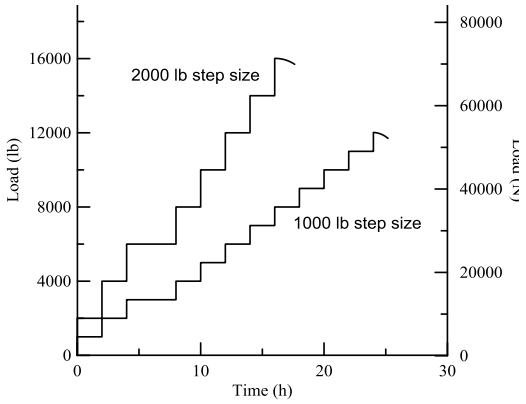

Figure 1: Load (lb) versus time (h) schematic for rising step load tests with 2000 lb (8,900 N) and 1,000 lb (4,450 N) step sizes and 2 h step times.

Single-edge notch bending,[23–26] single-edge notch tension,[27,28] and compact tension[29,30] specimens have all been used to determine K_{th} values in corrosive environments through fracture mechanics testing. Very thick specimens are required to achieve plane strain conditions when using these types of specimens due to the high toughness of alloy 718 and other nickel-base CRAs. An alternative specimen design for this type of testing is the circular notched tensile (CNT) specimen. The geometry of the CNT specimen results in a significantly smaller diameter to achieve plane strain conditions.[31] Also, it has been shown that fatigue pre-cracking may not be necessary if a sharp enough notch is machined in a CNT specimen.[31]

API[(3)] standard 6ACRA provides acceptable ranges for annealing and aging heat treatments for 718 in downhole environments, as well as examples of acceptable microstructures and acceptance criteria for room temperature mechanical properties such as yield strength, ultimate tensile strength, percent elongation, reduction in area, and hardness.[32] The heat treatments in the API 6ACRA standard are intended to achieve high-strength while also avoiding growth of δ phase at grain boundaries because δ phase can significantly increase susceptibility to intergranular cracking due to hydrogen embrittlement.[1,3,12–15] The acceptable heat treatment ranges for the 120 ksi (827 MPa) minimum yield strength and 140 ksi (965 MPa) minimum yield strength designations are shown in Table 1.[32] The heat treatments are based on previous research to determine optimal aging treatments for alloy 718 for use in oil and gas applications.[33] Annealing is performed above 1021 °C to ensure dissolution of δ and thereby increase hydrogen embrittlement resistance and the amount of niobium available for γ" precipitation.[34–37] In certain service conditions, 718 can experience hydrogen embrittlement despite being heat treated according to the API 6ACRA standard due to limited δ phase precipitation along grain boundaries;[3,4] these precipitates are formed during the aging step of the heat treatment.

Table 1
Allowable Heat Treatments for Alloy 718 given in API 6ACRA[32]

Alloy	Designation	Anneal Temperature (°C)	Anneal Time (h)	Age Temperature (°C)	Age Time (h)
718	120 ksi (827 MPa)	1021-1052	1.0-2.5	774-802	6-8
718	140 ksi (965 MPa)	1021-1052	1.0-2.5	760-802	6-8

(3) American Petroleum Institute (API), 1220 L St. N.W. Washington, DC 200005-0470

This paper evaluates the susceptibility of over-aged and peak-aged microstructures of alloy 718 to cathodic hydrogen embrittlement through in situ slow strain rate tensile testing and rising step load testing. Mechanical property ratios for slow strain rate tensile tests representing the susceptibility of each microstructure to hydrogen embrittlement are compared to the threshold stress intensity factors for crack growth (K_{th}) of specimens tested with cathodic polarization that are determined in RSL tests performed with different step times and step sizes. The fracture surfaces produced by each test method are also compared.

EXPERIMENTAL PROCEDURE

Alloy 718, with the composition given in Table 2, was hot-rolled to a plate with a thickness of 0.75 in (1.91 cm) and a width of approximately 9 in (23 cm). The plate was sectioned and furnace heat treated according to Table 3. The highest allowed annealing time and temperature within the guidelines of API standard 6ACRA (1050 °C for 2.5 h) was chosen to ensure maximum dissolution of δ phase produced during the previous thermomechanical processing. After annealing, the plates were water quenched to room temperature. Aging was performed to produce a peak-aged condition with the lowest aging temperature and time (760 °C, 6 h) and an over-aged condition with the highest aging temperature and time (800 °C, 8 h) allowed in API standard 6ACRA. The plates were air cooled after the aging step.

Table 2
Composition of Nickel-Base Corrosion Resistant Alloy 718

wt%	Ni	Cr	Nb	Mo	Ti	Al	Co
Alloy 718	53.39	18.44	5.00	2.87	1.02	0.52	0.33

C	Mn	Si	P	S	B	Cu	Fe
0.015	0.119	0.075	0.009	0.0004	0.003	0.10	17.99

The resulting grain sizes for each heat treatment, measured with the concentric circles method outlined in ASTM standard E112[38] are also given in Table 3. Metallographic samples of the two heat treatment conditions were prepared and evaluated through light optical microscopy and scanning electron microscopy. Intragranular carbides and grain boundary precipitates were identified with electron dispersive spectroscopy (EDS).

Table 3
Heat Treating Schedule and Resulting Grain Sizes for Alloy 718

Condition	Anneal Temperature (°C)	Anneal Time (h)	Age Temperature (°C)	Age Time (h)	Mean Intercept Length (μm)
Peak-aged	1050	2.5	760	6.0	129±5
Over-aged	1050	2.5	800	8.0	121±8

Subsize tensile and circular notch tensile (CNT) specimen blanks were machined from the plates in the longitudinal direction by electrical discharge machining. Subsize tensile specimens with a gauge length of 1.00 in (25.4 mm) and a gauge diameter of 0.15 in (3.81 mm), as specified in NACE TM0198, were machined from the blanks and polished to a surface finish of 10 μin (0.254 μm).[6] Circular notch tensile specimens were machined with a major diameter of 0.50 in (12.7 mm) and a diameter at the notch of 0.315 in (8.00 mm). The notch radius of the CNT specimens was 0.0034 in (0.086 mm) or less resulting in a stress concentration factor (K_t) of 6 or greater. CNT specimens with stress concentration factors of 6 or greater have been shown to produce fracture toughness values that are comparable to fracture toughness values from fatigue pre-cracked compact tension specimens.[31]

Rockwell C hardness of the two heat treatment conditions was performed according to ASTM E18.[39] Room temperature tensile tests were performed in air with the subsize tensile specimens and at an engineering strain rate of 5.0×10^{-4} s^{-1}. Charpy impact toughness tests were performed according to

ASTM E23 on standard size Charpy specimen type A with the notch machined in the longitudinal direction and at a temperature of -10 °C.[40] Candidate stress intensity factors for crack growth (K_Q) in air were determined by tensile tests of the CNT specimens at a constant displacement rate of 0.005 in/s (0.0127 cm/s).

Slow strain rate tensile tests were performed at an engineering strain rate of 1.0 x 10^{-6} s^{-1} on a tensile frame with a compliance of 22 MN/m. Three tests were performed in the ambient laboratory environment, and three tests were performed with cathodic polarization of the specimen in an acidic solution for each aging condition.

Rising step load tests were performed with either 1,000 lb (4,450 N) or 600 lb (2,670 N) step sizes and with either 2 h or 4 h step times on the peak-aged and over-aged conditions. According to ASTM F1624,[22] the initial step size should be 5% of the load to fracture when the specimen is pulled in tension at a constant displacement rate. The load for fracture for the peak-aged and over-aged conditions was determined by the tensile tests at a constant displacement rate of 0.005 in/s (0.0127 cm/s). The average load for fracture for the two conditions was approximately 20,000 lb (89,000 N), so the initial step size was chosen as 1,000 lb (4,450 N) (5% of 20,000 lb (89,000 N). The highest load for crack growth determined by the 1,000 lb (4,450 N) step size tests was 12,000 lb (53,400 N) so 600 lb (2,670 N) was chosen as the next step size to test (5% of 12,000 lb (53,400 N)). The step time of 4 h was chosen because 4 h is the longest step time used in ASTM F1624.[22] A step time of 2 h was tested to evaluate the effect of decreasing step time on K_{th}. The same step sizes and step times were used for the peak-aged and over-aged conditions to allow for a direct comparison of K_{th}.

A plot of load versus time from a rising step load test is shown in Figure 2 to demonstrate the methodology for determining K_{th}. The load decreased at a decreasing rate with time due to stress relaxation on every step before the onset of fracture as shown by the lowest step in Figure 2. When crack growth occurred, the load decreased at an increasing rate with time as shown by the highest step in Figure 2. The corresponding threshold load for crack growth, P_{th}, which was used to determine K_{th}, was chosen as the final load of the step before the onset of crack growth. K_{th} was calculated from P_{th} with equation (1), where D is the major diameter of the specimen and d is the diameter at the notch:[41]

$$K_{th} = \frac{P_{th}}{D^{3/2}}\left[1.72\left(\frac{D}{d}\right) - 1.27\right] \quad (1)$$

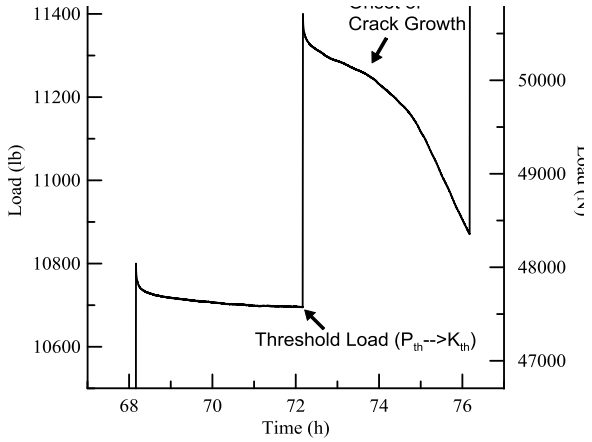

Figure 2: Load (lb) versus time (h) plot for rising step load test with 600 lb (2,670 N) steps and 4 h step times showing the step at which the onset of crack growth occurred and the load selected as the threshold load for crack growth (P_{th}).

All SSR and RSL cathodic polarization tests were performed in acrylic cells with a volume of 0.5 L; the cells were electrically isolated from the load frames. The cells were filled with 0.5 M H_2SO_4 and de-aerated with argon gas. The argon gas was bubbled through the solution at a rate of 1.0 ft^3/h (28 L/h) to stir the solution throughout the test. Cathodic polarization was performed at a current density of 5 mA/cm². Two iridium-tantalum oxide coated titanium anodes functioned as the counter electrodes and were positioned on opposite sides of the specimen. The electrochemical potential was monitored with a saturated calomel reference electrode.

Images of the fracture surfaces were taken with a Nikon D70[†] camera after cleaning with methanol. The fracture surfaces were also evaluated in an FEI Quanta 600i[†] environmental scanning electron microscope (ESEM) and a JEOL 7000[†] field emission scanning electron microscope (FESEM). Secondary electron imaging was performed at a voltage of 20 kV.

RESULTS AND DISCUSSION

The peak-aged and over-aged conditions had similar grain sizes with a mean intercept length of 129 µm for the peak-aged condition and 121 µm for the over-aged condition. SEM evaluation of grain boundaries revealed small δ phase precipitates in the peak-aged and over-aged conditions as shown in the SEM images in Figure 3. The δ phase precipitates were present at many more grain boundaries and were much larger for the over-aged condition than the peak-aged condition. δ phase composition was confirmed through EDS analysis. Larger γ' and γ" precipitates were also visible in the over-aged condition compared to the peak-aged condition.

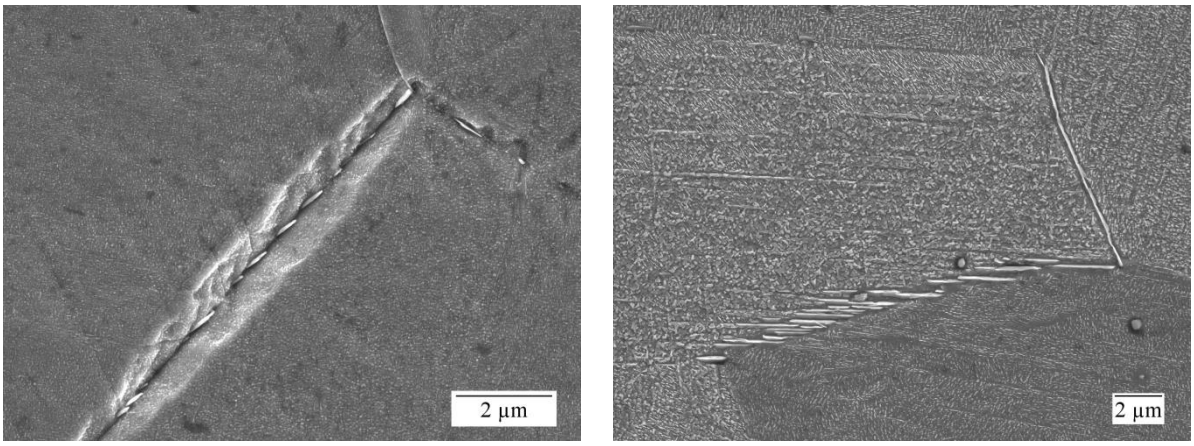

(a) (b)

Figure 3: SEM images of grain boundary δ phase precipitates in (a) peak-aged and (b) over-aged alloy 718.

Table 4 provides Rockwell C hardness values, room temperature tensile mechanical property results, Charpy impact toughness testing results, and candidate stress intensity factors (K_Q) for both heat treatment conditions. In addition to having a higher strength, the peak-aged condition exhibited higher impact toughness and fracture toughness than the over-aged condition.

Table 4
Rockwell C Hardness, Room Temperature Tensile, Charpy Impact, and K_Q Testing Results for Alloy 718

Condition	Hardness (HRC)	0.2% Yield Stress (MPa)	UTS (MPa)	Total Elongation (%)	Impact Toughness (J)	K_Q ($MPa*m^{1/2}$)
Peak-aged	39.0±0.4	989±0	1256±6	30.3±0.7	112±3	95.8
Over-aged	35.0±0.5	757±16	1150±11	31.1±1.0	85±2	82.9

[†]Trade name.

The averages of the mechanical property results from the SSR tests performed in air and with cathodic polarization (CP) for the peak-aged and over-aged conditions are given in Table 5. Figure 4 shows stress-strain curves for the peak-aged and over-aged conditions. The total elongation, yield stress, ultimate tensile stress (UTS), and reduction in area ratios between the cathodic polarization condition and the ambient environment for both microstructural conditions are given in Table 6. Ductility, as represented by total elongation and reduction in area, was reduced by hydrogen charging for both microstructural conditions. The yield strength ratios for both conditions were above 99%, indicating that hydrogen had little or no effect on the stress required to initiate plastic deformation.

The over-aged condition exhibited a greater total elongation ratio (18.7%) and reduction in area ratio (30.8%) than the peak-aged condition (12.1% total elongation ratio and 26.4% reduction in area ratio) despite the over-aged condition having a greater amount of δ phase precipitation on grain boundaries. On the other hand, the ultimate tensile strength ratio for the over-aged condition (81.2%) was lower than the ultimate tensile strength ratio for the peak-aged condition because of the higher work hardening rate for the over-aged condition. The loss of plastic deformation due to premature failure in hydrogen prevented the greater increase in stress from work hardening that the over-aged condition experiences compared to the peak aged condition.

Table 5
Strength and Ductility Results from SSR Tests in Air and with Cathodic Polarization (CP) for Alloy 718

Condition	Environment	0.2% Yield Stress (MPa)	UTS (MPa)	Total Elongation (%)	Reduction in Area (%)
Peak-aged	Air	1,006±11	1,253±13	28.9±1.6	32.8±2.3
Peak-aged	CP	1,000±14	1,104±8	3.50±0.6	8.7±0.2
Over-aged	Air	769±14	1,166±9	31.2±2.1	32.3±2.8
Over-aged	CP	765±12	947±19	5.83±0.7	9.9±0.4

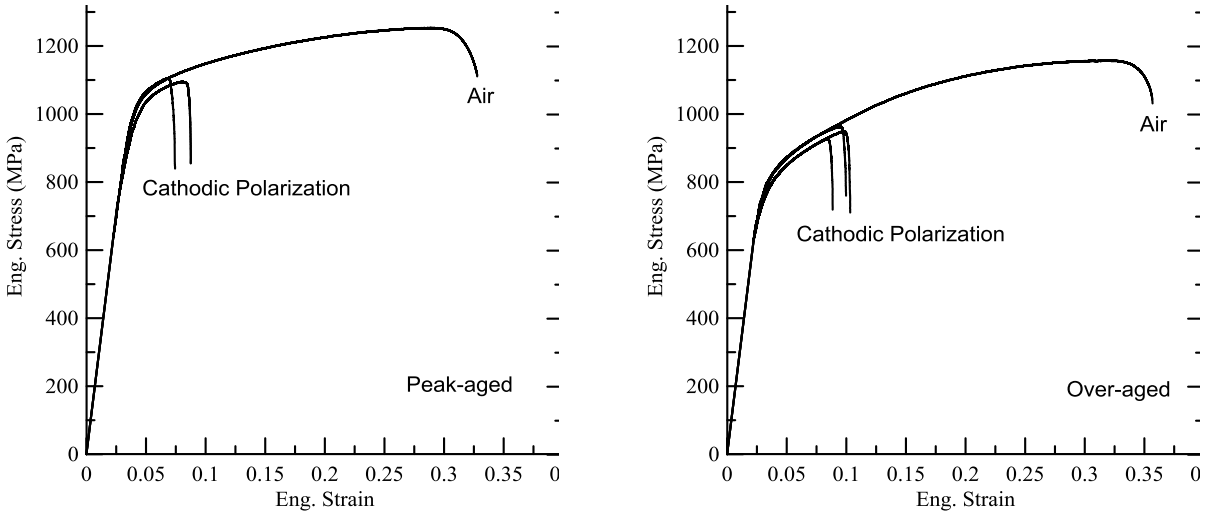

(a) (b)

Figure 4: Engineering stress versus engineering strain curves for slow strain rate tensile tests in air and under cathodic polarization (CP) for alloy 718 in the (a) peak-aged and (b) over-aged conditions. Only one representative stress-strain curve is shown for air.

Table 6
Mechanical Property Ratios for SSR and RSL Tests with Cathodic Polarization Versus Ambient Environment for Alloy 718

Condition	Total Elongation (%)	0.2% Yield Stress (%)	UTS (%)	Reduction in Area (%)	K Ratio (%)
Peak-Aged	12.1±2.1	99.4±1.8	88.1±1.1	26.4±1.9	43.4±2.7
Over-Aged	18.7±2.7	99.5±2.5	81.2±1.7	30.8±2.9	57.5±3.3

Load versus time curves from RSL testing under cathodic polarization are shown in Figure 5 for the peak-aged and over-aged conditions. Each curve is labeled with the step size and step time with which the test was performed, and the arrows indicate the step at which crack growth began. The effect of step time varied for the two conditions. For the over-aged condition with 1,000 lb (4,450 N) and 600 lb (2,670 N) step sizes and the peak-aged condition with the 1,000 lb (4,450 N) step size, there was no effect of step time on the step at which crack growth occurred. For the peak-aged condition with 600 lb (2,670 N) step sizes, crack growth began one step earlier for the test with 4 h step times (10,200 lb (45,400 N)) than the test with 2 h step times (10,800 lb (48,000 N)).

Changing the step size had a more consistent effect on the RSL results. Decreasing the step size resulted in crack growth occurring at a lower load for every combination of aging condition and step time. However, crack growth at a lower load for the 600 lb (2,670 N) step sizes does not necessarily result in a lower K_{th} because K_{th} is determined by the final load of the previous step. For example, if crack growth occurred at the 11,000 lb (48,900 N) step for 1,000 lb (4,450 N) step sizes, then the step for determining K_{th} would be the 10,000 lb (44,500 N) step and if crack growth occurred at the 10,800 lb (48,000 N) step for 600 lb (2,670 N) step sizes, then the step determining K_{th} would be the 10,200 lb (45,400 N) step. A higher K_{th} would result from the 10,200 lb (45,400 N) force used for the calculation with the 600 lb (2,670 N) step size than the 10,000 lb (44,500 N) force used for the calculation with the 1,000 lb (4,450 N) step size.

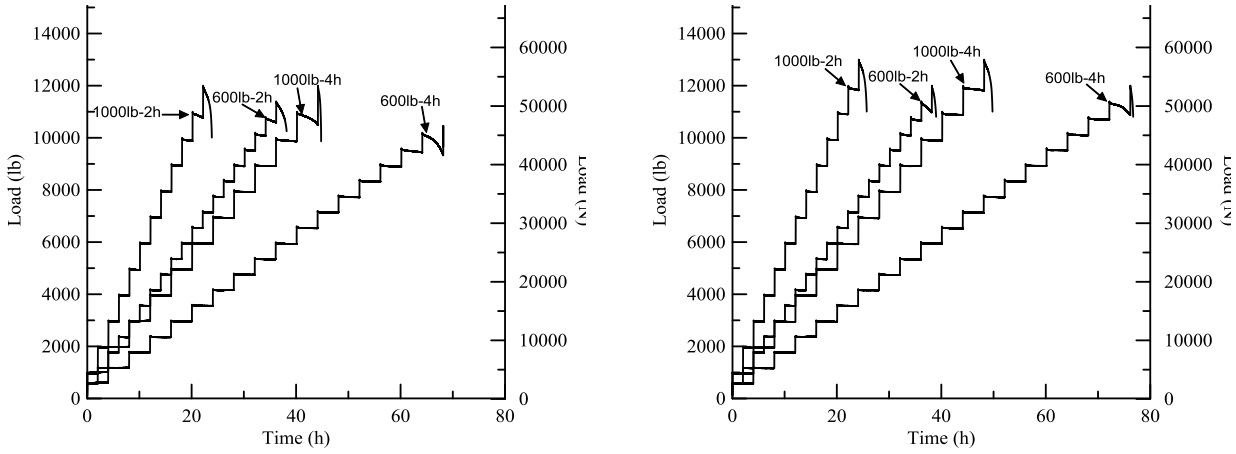

Figure 5: Load (lb) versus time (h) plots for RSL tests of alloy 718 in the (a) peak-aged and (b) over-aged conditions under cathodic polarization. Each curve is labeled with the programmed step size and step time. The arrows indicate the step at which crack growth began for each test.

The load versus time curves from Figure 5 are re-plotted with step sizes of 1,000 lb (4,450 N) in Figure 6a and step sizes of 600 lb (2,670 N) in Figure 6b to show differences between the peak-aged and over-aged conditions. Crack growth began in the peak-aged condition one step before crack growth began in the over-aged condition for the 1,000 lb (4,450 N)-4 h, 1,000 lb (4,450 N)-2 h, and 600 lb (2,670 N)-2 h combinations of step size and step time. For the 600 lb (2,670 N)-4 h combination, crack growth began in the peak-aged condition two steps before crack growth began in the over-aged condition. The higher measured K_{th} of the over-aged condition at all step sizes and step times shows that the peak-aged condition was more severely embrittled when tested with cathodic polarization even though the over-aged condition had a lower K_Q in air and a lower Charpy impact toughness. K ratios, which are defined as the lowest K_{th} from the RSL tests under cathodic polarization for each condition divided by the K_Q determined by the constant displacement rate test of the CNT specimen in air, are given in Table 6. The higher K ratio of the over-aged condition (57.5 %) compared to the peak-aged condition (43.4 %) corresponds with the larger total elongation and reduction in area ratios of the over-aged condition from the SSR tests. Again, the over-aged condition was more resistant to hydrogen embrittlement despite having greater amounts of δ phase precipitation on grain boundaries.

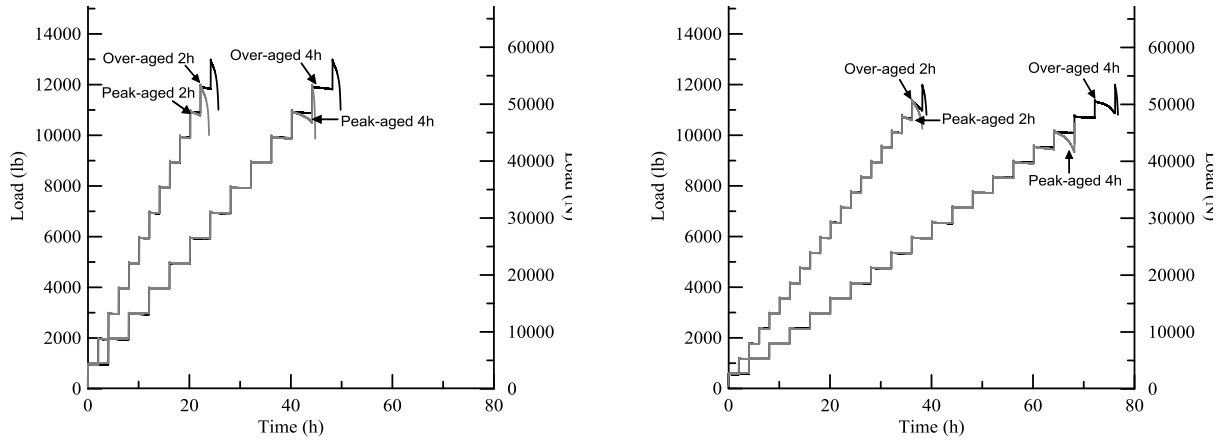

(a) (b)

Figure 6: Load (lb) versus time (h) plots for RSL tests of peak-aged and over-aged alloy 718 with step sizes of (a) 1,000 lb (4,450 N) and (b) 600 lb (2,670 N). Each curve is labeled with the aging condition and step time. The arrows indicate the step for crack growth for each test.

Table 7 shows the initial load of the step at which crack growth occurred and the resulting K_{th} for all RSL tests of the peak-aged and over-aged conditions. Even though K_{th} is determined by the load at the end of the same step for many of the tests, small differences in K_{th} occur due to different amounts of stress relaxation and small differences in specimen dimensions. The tests with step sizes of 600 lb (2,670 N) have less uncertainty than the tests with step sizes of 1,000 lb (4,450 N). The uncertainty of K_{th} can be no less than plus or minus the change in K_{th} produced by each increase in load, so smaller step sizes result in smaller uncertainties.

A study by Kernion *et al.* also examined the effect of changing step time on RSL results of alloy 718 using 4 point bend specimens with different microstructures, though the polarization potential was also varied simultaneously.[23] A voltage of -1.1 V versus SCE (saturated calomel electrode) with 3.5 h step times was used to simulate galvanic coupling and a voltage of -1.4 V versus SCE with 1 h step times was used to determine if higher voltages with longer step times could accelerate the test while achieving the same K_{th} values. Lower K_{th} values were produced with the -1.4 V/ 1 hr combination, which shows that the higher potential lowered the K_{th} values despite the shorter step times. This study also found a peak-aged condition to have a lower K_{th} than an over-aged condition under cathodic polarization, consistent with the results of the present study.

Table 7
Rising Step Load Test Results for Alloy 718 Tested With Cathodic Polarization

Condition	Step Size (lb (N))	Step Time (h)	Initial Load of Crack Growth Step (lb (N))	K_{th} (MPa*$m^{1/2}$)
Over-aged	1,000 (4,450)	4	12,000 (53,400)	50.0±4.6
Over-aged	1,000 (4,450)	2	12,000 (53,400)	49.8±4.6
Over-aged	600 (2,670)	4	11,400 (50,700)	49.1±2.8
Over-aged	600 (2,670)	2	11,400 (50,700	47.7±2.7
Peak-aged	1,000 (4,450)	4	11,000 (48,900)	44.6±4.5
Peak-aged	1,000 (4,450)	2	11,000 (48,900)	44.9±4.5
Peak-aged	600 (2,670)	4	10,200 (45,400)	42.9±2.7
Peak-aged	600 (2,670)	2	10,800 (48,000)	45.2±2.7

In the present study, the fracture surfaces of the peak-aged and over-aged SSR specimens tested in air were ductile as shown by the macrophotograph of the fracture surface of the peak-aged specimen in Figure 7a. A macrophotograph of the fracture surface of an over-aged alloy 718 CNT specimen after a constant displacement rate test to failure in air is shown in Figure 7b. The fracture surfaces of the CNT specimens of both conditions tested in air consisted of a combination of intergranular fracture and ductile microvoid coalescence. The brittle fracture surface features are a result of the stress triaxiality introduced by the notch.

Both conditions exhibited both brittle and ductile fracture features after SSR testing with cathodic polarization. Brittle cracks initiated at the surface and extended into the material until the fracture mechanism transitioned to ductile microvoid coalescence at the interior of the specimen. Figure 8a shows a macrophotograph of the fracture surface of the over-aged condition SSR tested in the cathodic hydrogen charging environment; the fracture surface contains a ductile region of microvoid coalescence (MVC) and a brittle region composed of intergranular cracking (IGC) and transgranular cracking (TGC). Intergranular cracking in the brittle fracture region of an over-aged specimen tested in hydrogen is also clearly visible in the SEM image in Figure 8b.

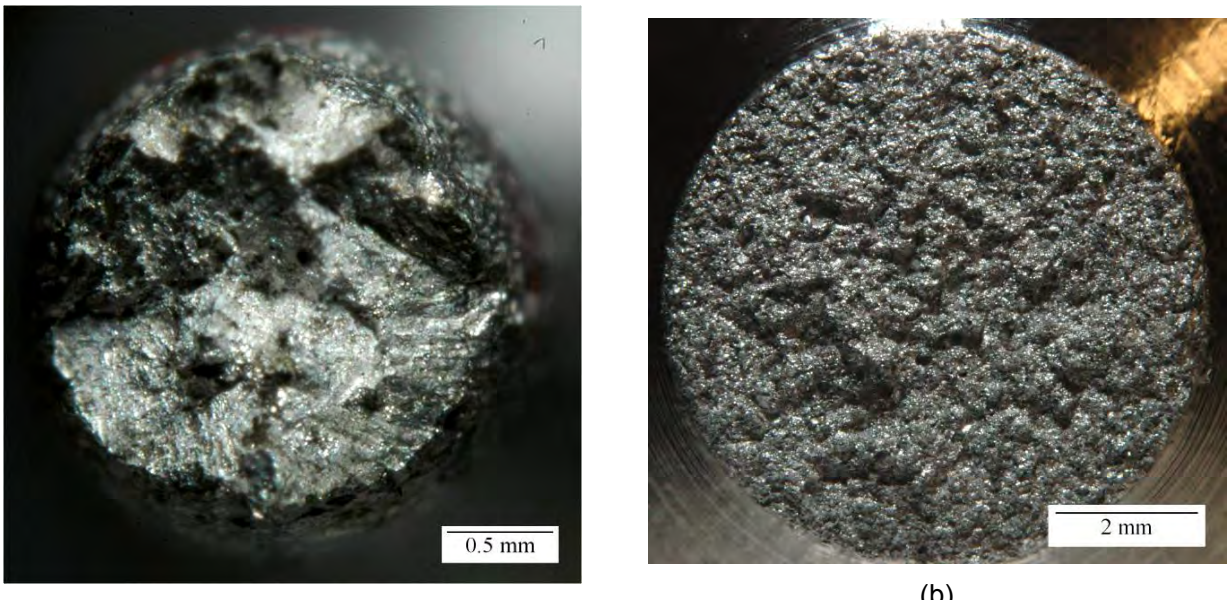

(a) (b)

Figure 7: (a) Macrophotograph of the fracture surface of peak-aged alloy 718 after slow strain rate testing to failure in air and (b) macrophotograph of the fracture surface of over-aged alloy 718 CNT specimen after constant displacement rate testing to failure in air.

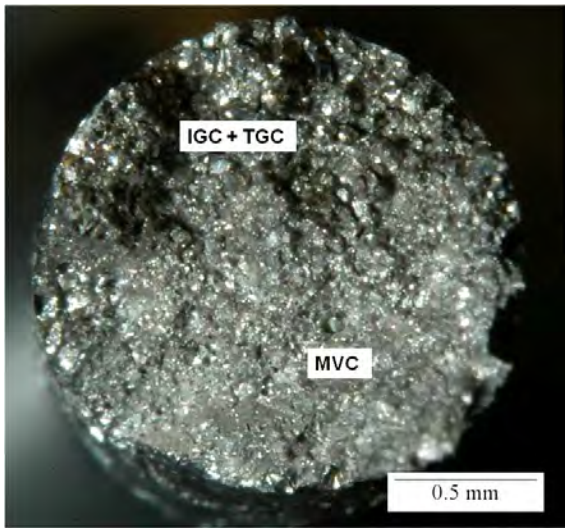

(a)

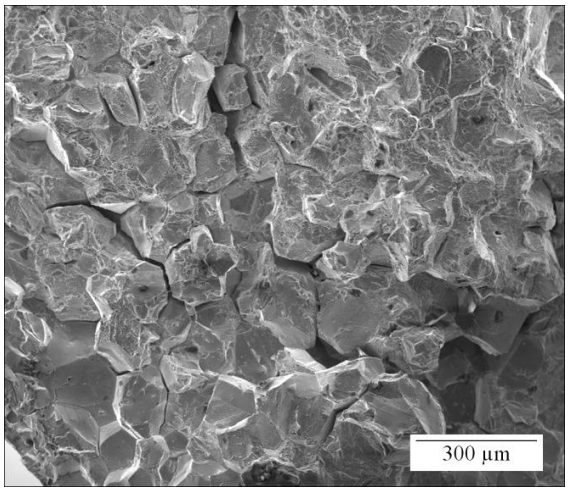

(b)

Figure 8: (a) Macrophotograph of the fracture surface of the over-aged alloy 718 SSR tested under cathodic polarization showing regions of intergranular cracking (IGC), transgranular cracking (TGC), and ductile microvoid coalescence (MVC) (b) SEM image of brittle fracture region of the over-aged alloy 718 tested under cathodic polarization.

RSL testing while cathodically charging the specimens produced a ring of brittle fracture starting at the notch and extending toward the center of the specimen for both the peak-aged and over-aged conditions. A macrophotograph of the fracture surface of the peak-aged condition after RSL testing under cathodic polarization is shown in Figure 9a. The fracture transitioned to ductile microvoid coalescence at the center of the specimen, but the area of ductile fracture was not always centered at the middle of the specimen because the depth of brittle fracture was not always uniform around the perimeter of the specimen. The transition from brittle to ductile fracture is shown in the SEM image of the fracture surface of the over-aged condition in Figure 9b.

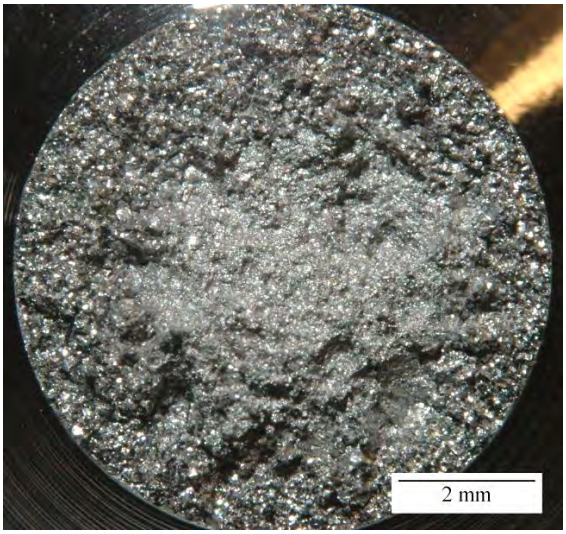

(a)

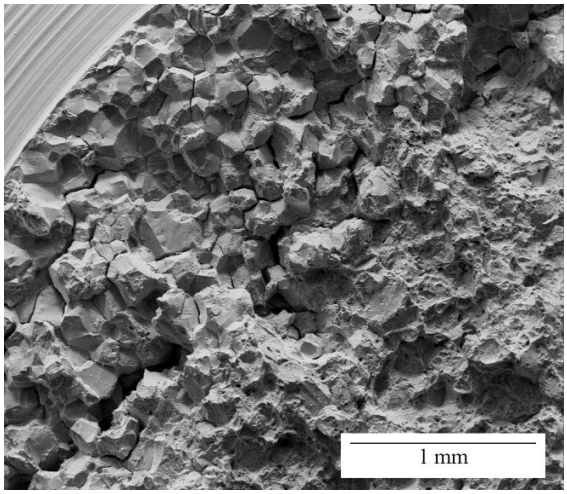

(b)

Figure 9: (a) Macrophotograph of the fracture surface of the over-aged condition of alloy 718 RSL tested under cathodic polarization and (b) SEM image of transition from brittle fracture region to ductile fracture region of over-aged alloy 718 tested under cathodic polarization.

Transgranular cracking in the brittle regions of both conditions resembled cleavage on specific crystallographic planes. The cleavage cracking would sometimes have visible river marks and would normally begin and end at either a grain boundary or an annealing twin. SEM images of combinations of transgranular cracking and intergranular cracking are shown for the peak-aged condition after SSR testing in Figure 10a and after RSL testing in Figure 10b. Cleavage cracking was sporadically located in the brittle regions. Fracture features that appeared as deviations from the intergranular crack path were also visible on the smooth intergranular cracking areas in both conditions. These fracture features can be seen in the SEM images of the peak-aged condition after RSL testing in Figure 11a and the over-aged condition after SSR testing in Figure 11b.

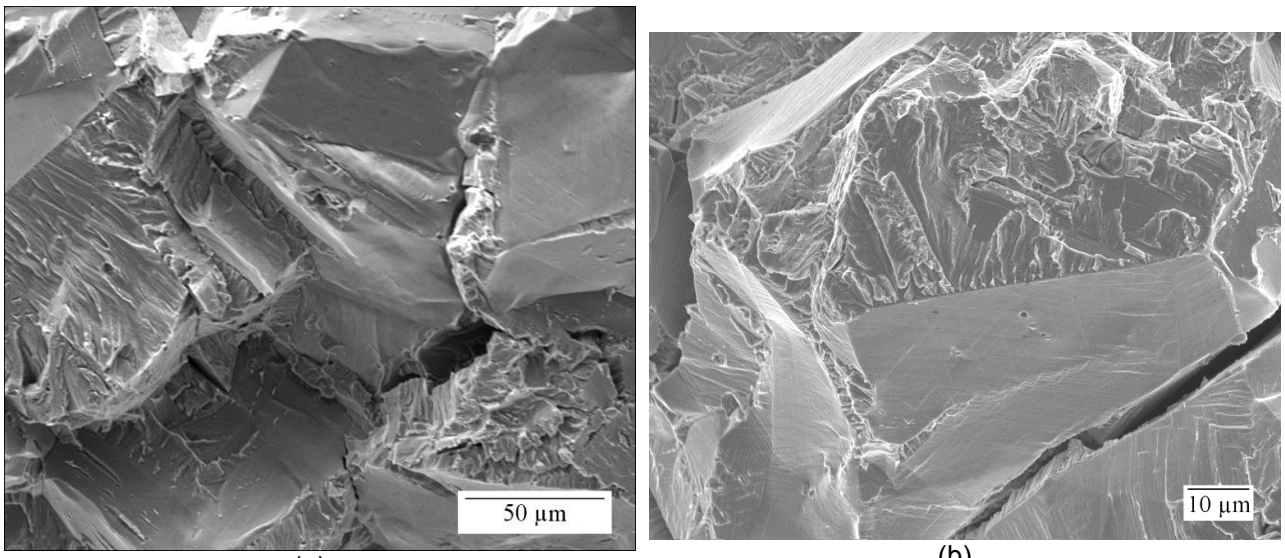

(a) (b)

Figure 10: SEM images of transgranular cracking (TGC) that occurred along specific crystallographic planes mixed with intergranular cracking (IGC) from (a) SSR test and (b) RSL test with cathodic polarization of peak-aged alloy 718.

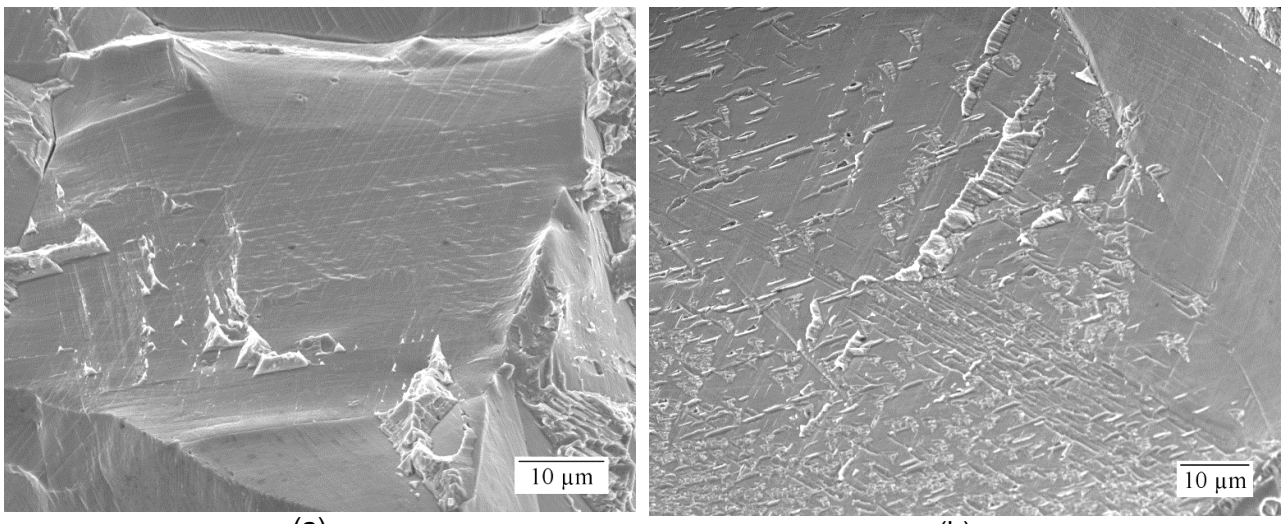

(a) (b)

Figure 11: SEM images of small deviations from the intergranular crack path from (a) RSL test with cathodic polarization of peak-aged alloy 718 and (b) SSR test with cathodic polarization of over-aged alloy 718.

Peak-aged alloy 718 was more susceptible to hydrogen embrittlement than over-aged alloy 718 in both the SSR and RSL tests, even though there was less δ phase present at the grain boundaries in the peak-aged condition. Since δ phase precipitation has been shown to increase hydrogen embrittlement susceptibility,[1,3,12–15] it is possible that differences in size and coherency of the γ' and γ" precipitates, the primary strengthening phases of alloy 718, improve the hydrogen embrittlement resistance of over-aged alloy 718 relative to the peak-aged condition. Despite differences in SSR and RSL performance, the fracture appearance of the over-aged and peak-aged conditions exhibited similar features in the embrittled regions (smooth intergranular cracking, transgranular cleavage cracking, small deviations from the intergranular crack path).

The over-aged and peak-aged conditions exhibited the same relative performance in both the SSR and RSL tests even though the tests evaluate different aspects of crack initiation and growth. SSR testing of smooth specimens requires crack initiation on the surface of the specimen and then crack growth until failure; however, the environmental effect on crack initiation and crack growth cannot be distinguished by the SSR test because the point at which cracks initiate in the SSR test is unknown. Also, the higher strength of the peak aged condition means the stress on a crack is higher during plastic deformation than for the over-aged condition, making it difficult to evaluate if the greater ductility loss than the over-aged condition is due to microstructural factors. On the other hand, the RSL test only evaluates resistance to crack growth without extensive plasticity outside of the notched region and definitively showed an influence of microstructure on the K_{th} value. Both testing methodologies produced hydrogen cracks consisting of predominantly intergranular cracking with some crystallographic transgranular cracking for both heat treatment conditions. Similarities in fracture mode between the two types of mechanical tests show that the mechanisms for crack propagation were possibly similar despite different loading conditions. In the SSR test, crack growth occurs while the gauge undergoes uniform plastic deformation, while in the RSL test, plastic deformation only occurs in the plastic zone ahead of the notch tip. The similarity in fracture mode may indicate that fracture mode due to hydrogen embrittlement is independent of the amount of plasticity around a growing crack or that the uniform plastic deformation in the SSR test and the plastic zone in the RSL test played comparable roles in the fracture mechanism.

SUMMARY AND CONCLUSIONS

Slow strain rate (SSR) tensile tests of smooth specimens and rising step load (RSL) tests of circular notched tensile specimens were performed on peak-aged and over-aged conditions of alloy 718 in air and under cathodic polarization to simulate hydrogen embrittlement in oil and gas environments. The results from each test were consistent in that the over-aged condition had higher total elongation and reduction in area ratios from SSR testing and higher K_{th} values from RSL testing than the peak-aged condition despite more δ precipitation on grain boundaries in the over-aged condition. These results suggest that the differences in γ' and γ'' precipitation between the conditions affects hydrogen embrittlement susceptibility. Smaller step sizes for the RSL tests resulted in lower K_{th} values with less uncertainty for both conditions at all step times studied. Differences in step time only resulted in a change in the step at which crack growth occurred for the peak-aged condition tested with a 600 lb (2,670 N) step size. Combinations of intergranular and transgranular cracking were present in the brittle hydrogen affected regions on the fracture surfaces of both conditions after SSR and RSL testing with cathodic polarization.

ACKNOWLEDGEMENTS

The authors gratefully acknowledge the support of the Advanced Steel Processing and Products Research Center at the Colorado School of Mines as well as the experimental and material support of the Special Metals Corporation and Chevron Corporation.

REFERENCES

1. S. Huizinga, B. McLoughlin, J. Jong, and W. Liek, “Offshore Nickel Alloy Tubing Hanger and Duplex Stainless Steel Piping Failure Investigations,” *Corrosion*, 2003, no. 03129, pp. 1–9.
2. S. Shademan, J. Martin, and A. Davis, “UNS N07725 Nickel Alloy Connection Failure,” *Corrosion*, 2012, pp. 1–23.
3. T. Cassagne, M. Bonis, D. Hillis, and C. Duret, “Understanding Field Failures of Alloy 718 Forging Materials in HP/HT wells,” *Eurocorr*, 2008, pp. 1–13.
4. P. I. Nice, E. Piccolo, R. Morana, and L. Scoppio, “Corrosion Evaluation of Temporarily Installed ‘Well Zone Isolation Equipment’ after Long Term Exposure to a Caesium Formate Mud System in a North Sea HPHT Well,” in *Corrosion*, 2013, no. 2313, pp. 1–15.
5. E. Piccolo, P. I. Nice, O. Fattnes, R. Morana, A. Bufalini, A. Lucci, and L. Scoppio, “High Pressure High Temperature Testing of PH Nickel Alloy and Super Martensitic Stainless Steel in Cesium Formate Completion Fluid,” *Corrosion*, 2012, pp. 1–12.
6. NACE TM0198 (latest revision), “Slow Strain Rate Test Method for Screening Corrosion Resistant Alloys (CRAs) for Stress Corrosion Cracking in Sour Oilfield Service” (Houston, TX: NACE).
7. ASTM G129 (latest revision), “Standard Practice for Slow Strain Rate Testing to Evaluate the Susceptibility of Metallic Materials to Environmentally Assisted Cracking” (West Conshohocken, PA: ASTM).
8. P. R. Rhodes, “Environment-Assisted Cracking of Corrosion-Resistant Alloys in Oil and Gas Production Environments: A Review,” *Corrosion*, vol. 57, no. 11, pp. 923–966, Nov. 2001.
9. L. Foroni and C. Malara, “Hydrogen Embrittlement Susceptibility of Precipitation Hardened Ni-Alloys,” *Corrosion*, no. 3948, pp. 1–15, 2014.
10. W. Huang, W. Sun, A. Samson, D. Muise, and C. Haarseth, “Investigation of Hydrogen Embrittlement Susceptibility of Precipitation Hardened Nickel Alloys Under Cathodic Protection Condition,” *Corrosion*, 2014.
11. P. Nice, G. Rorvik, R. Strong, J. H. Olsen , W. M. Bailey, and T. G. Mobberley, “Hydrogen Embrittlement Failure of a Precipitation Hardened Nickel Alloy Subsurface Safety Valve Component Installed in a North Sea Seawater Injection Well,” *Corrosion*, no. 3892, pp. 1–16, 2014.
12. F. Pires, R. Clements, F. Santos, J. Clevelario, and T. Sheldrake, “Evaluation of the Performance of Inconel 718 Fasteners Subjected to Cathodic Protection Systems in Offshore and Subsea Applications,” *ASME 30th International Conference on Ocean, Offshore and Arctic Engineering*, 2011, pp. 165–172.
13. T. S. Rosa, A. F. Ribeiro, L. H. de Almeida, and D. S. dos Santos, “Effects of the Microstructure on the Hydrogen Diffusivity in Ni-Based Superalloy 718,” *Defect and Diffusion Forum*, vol. 297–301, pp. 733–738, Apr. 2010.
14. L. Liu, C. Zhai, C. Lu, W. Ding, A. Hirose, and K. F. Kobayashi, “Study of the effect of δ phase on Hydrogen Embrittlement of Inconel 718 by Notch Tensile Tests,” *Corrosion Science*, vol. 47, no. 2, pp. 355–367, Feb. 2005.
15. L. Liu, K. Tanaka, A. Hirose, and K. F. Kobayashi, “Effects of Precipitation Phases on the Hydrogen Embrittlement Sensitivity of Inconel 718,” *Science and Technology of Advanced Materials*, vol. 3, no. 4, pp. 335–344, Dec. 2002.
16. L. Fournier, D. Delafosse, and T. Magnin, “Cathodic Hydrogen Embrittlement in Alloy 718,” *Materials Science and Engineering: A*, vol. 269, no. 1–2, pp. 111–119, Aug. 1999.
17. I. Roy, M. Marya, D. Susnitzky, and H. Deng, “Comparative Performance of Three High-Strength Ni-Cr-Mo Alloys in Oilfield Simulated H_2S Environment,” *Materials Science Forum*, vol. 783–786, pp. 1857–1862, May 2014.
18. S. K. Mannan, E. Hibner, and B. Puckett, “Physical Metallurgy of Alloys 718, 725,725HS, 925 for Service in Aggressive Corrosive Environments.” 2003.
19. S. A. McCoy, S. K. Mannan, C. S. Tassen, D. Maitra, and J. R. Crum, “Investigation of the Effects of Hydrogen on High Strength Precipitation Hardened Nickel Alloys for O&G Service,” *Corrosion*, 2015, no. 5911.

20. D. McIntyre, R. Kane, and S. Wilhelm, “Slow Strain Rate Testing for Materials Evaluation in High-Pressure H2S Environments,” *Corrosion*, pp. 920–926, 1988.
21. R. Gangloff and B. Somerday, *Gaseous Hydrogen Embrittlement of Materials in Energy Technologies*. 2012.
22. ASTM F1624 (latest revision), “Standard Test Method for Measurement of Hydrogen Embrittlement Threshold in Steel by the Incremental Step Loading Technique” (West Conshohocken, PA: ASTM).
23. S. J. Kernion, J. H. Magee, T. N. Werley, P. B. Maxwell, and B. P. Somerday, “Measurement of Hydrogen Embrittlement Resistance of Alloy 718 and Custom Age 625 Plus Using the Rising Step Load Technique,” *8th International Symposium on Superalloy 718 and Derivatives*, 2014, pp. 579–591.
24. S. J. Kernion, K. A. Heck, J. H. Magee, and T. N. Werley, “Effect of Microstructure and Processing on the Hydrogen Embrittlement of Ni-base Superalloys,” *Corrosion*, 2015, no. 6053, pp. 1–12.
25. P. Tyler, M. Levy, and L. Raymond, “Investigation of the Conditions for Crack Propagation and Arrest Under Cathodic Polarization by Rising Step Load Bend Testing,” *Corrosion*, vol. 47, no. 2, pp. 82–87, 1991.
26. E. U. Lee, R. Goswami, M. Jones, and a. K. Vasudevan, “Environment-Assisted Cracking in Custom 465 Stainless Steel,” *Metallurgical and Materials Transactions A*, vol. 42, no. 2, pp. 415–423, Sep. 2010.
27. J. Lillard, R. Kelly, and R. Gangloff, “Effect of Electrode Potential on Stress Corrosion Cracking and Crack Chemistry of a Nickel-Base Superalloy,” in *Corrosion*, 1997.
28. Y. Lee and R. P. Gangloff, “Measurement and Modeling of Hydrogen Environment–Assisted Cracking of Ultra-High-Strength Steel,” *Metallurgical and Materials Transactions A*, vol. 38, no. 13, pp. 2174–2190, Mar. 2007.
29. K. A. Nibur, B. P. Somerday, C. S. Marchi, J. W. Foulk, M. Dadfarnia, and P. Sofronis, “The Relationship Between Crack-Tip Strain and Subcritical Cracking Thresholds for Steels in High-Pressure Hydrogen Gas,” *Metallurgical and Materials Transactions A*, vol. 44, no. 1, pp. 248–269, Nov. 2012.
30. W. Dietzel and J. Mueller-Roos, “Experience with Rising Load/Rising Displacement Stress Corrosion Cracking tTesting,” *Materials Science*, vol. 37, no. 2, pp. 107–112, 2001.
31. J. A. Lee, “Rapid and Low Cost Method to Determine the Plane Strain Fracture Toughness (KIc) in Hydrogen,” in *International Hydrogen Conference*, 2012, pp. 461–469.
32. API 6ACRA (latest revision), “Age-hardened Nickel-based Alloys for Oil and Gas Drilling and Production Equipment” (Washington, DC: API).
33. R. B. Bhavsar, A. Collins, and S. Silverman, “Use of Alloy 718 and 725 in Oil and Gas Industry,” *Superalloys 718, 625, 706 and Various Derivatives,* 2001, pp. 47–55, 2001.
34. X. Wei, W. Zheng, Z. Song, T. Lei, Q. Yong, and Q. Xie, “Elemental Partitioning Characteristics of Equilibrium Phases in Inconel 718 Alloy at 600–1100 °C,” *Journal of Iron and Steel Research, International*, vol. 20, no. 6, pp. 88–94, Jun. 2013.
35. X. Xie, C. Xu, G. Wang, J. Dong, W. Cao, and R. Kennedy, “TTT Diagram of a Newly Developed Nickel-Base Superalloy - ALLVAC 718 Plus,” *Superalloys 718, 625, 706 and Derivatives*, pp. 193–202, 2005.
36. D. Cai, W. Zhang, P. Nie, W. Liu, and M. Yao, “Dissolution Kinetics of δ Phase and its Influence on the Notch Sensitivity of Inconel 718,” *Materials Characterization*, vol. 58, pp. 220–225, 2007.
37. S. Azadian, L. Wei, and R. Warren, “Delta Phase Precipitation in Inconel 718,” *Materials Characterization*, vol. 53, pp. 7–16, 2004.
38. ASTM E112 (latest revision), “Standard Test Methods for Determining Average Grain Size” (West Conshohocken, PA: ASTM).
39. ASTM E18 (latest revision), “Standard Test Methods for Rockwell Hardness of Metallic Materials” (West Conshohocken, PA: ASTM).
40. ASTM E23 (latest revision), “Standar Test Methods for Notched Bar Impact Testing of Metallic Materials” (West Conshohocken, PA: ASTM).
41. G. Dieter, *Mechanical Metallurgy*, 3rd ed. McGraw-Hill, 1986.